How rigid are viruses

R. D. Hartschuh,[1] S. P. Wargacki,[2] H. Xiong,[1] J. Neiswinger,[1] A. Kisliuk,[1] S. Sihn,[3] V. Ward,[4] R. A. Vaia,[2] and A. P. Sokolov[1,*]

[1]*Department of Polymer Science, University of Akron, Akron, Ohio 44325, USA*

[2]*Materials and Manufacturing Directorate, Air Force Research Laboratory, Wright Patterson Air Force Base, Ohio 45433, USA*

[3]*Multi-Scale Composites & Polymers Division, University of Dayton Research Institute, 300 College Park, Dayton, Ohio 45469-0060, USA*

[4]*Department of Microbiology, Otago School of Medical Sciences, University of Otago, Dunedin, New Zealand*

(Received 6 January 2008; revised manuscript received 21 April 2008; published 15 August 2008)

Viruses have traditionally been studied as pathogens, but in recent years they have been adapted for applications ranging from drug delivery and gene therapy to nanotechnology, photonics, and electronics. Although the structures of many viruses are known, most of their biophysical properties remain largely unexplored. Using Brillouin light scattering, we analyzed the mechanical rigidity, intervirion coupling, and vibrational eigenmodes of *Wiseana iridovirus* (WIV). We identified phonon modes propagating through the viral assemblies as well as the localized vibrational eigenmode of individual viruses. The measurements indicate a Young's modulus of ~7 GPa for single virus particles and their assemblies, surprisingly high for "soft" materials. Mechanical modeling confirms that the DNA core dominates the WIV rigidity. The results also indicate a peculiar mechanical coupling during self-assembly of WIV particles.

DOI: 10.1103/PhysRevE.78.021907 PACS number(s): 87.16.dm, 87.80.Ek, 62.25.Fg, 63.22.Kn

I. INTRODUCTION

Viruses are traditionally considered infectious agents that hijack cellular function, causing mutation of genetic material for their own reproduction. New technologies, however, are finding ways to harness the amazing diversity and functionality of these well-organized and repetitive structures. The packaging and release mechanisms of the capsid shells, as well as the monodispersity, shape, size, and multivalent, site-specific surface functionality, make them attractive for a broad array of technologies, ranging from targeted drug delivery and gene therapy to templates for complex photonic and electronic materials [1–6]. For example, helical viruses such as tobacco mosaic virus and M13 bacteriophage offer controlled, uniform anisotropy, an elusive characteristic for nanoparticles, and have been shown as useful templates for metallic and semiconducting nanowires and as scaffolds for nanoparticle arrays with potential as data storage devices [7] and batteries [8,9]. The structures of many viruses are known through the use of x-ray crystallography and cryoelectron microscopy reconstruction. However, the proper use of viruses for various technologies depends on a number of characteristics, including the mechanical properties of the building blocks and their assembly. As a template for material synthesis, the mechanical properties ultimately determine the particle stability and durability, and thus define the useful process and performance window of these biological colloids and their assemblies. Biologically, mechanical characteristics of viral capsids influence morphological changes that occur during cellular infection. The virus particle is a metastable structure that must survive transmission between hosts, yet be capable of uncoating its genetic material upon infection. Receptor binding or changes between extra- and intracellular environments, such as *p*H, cause conformational changes of the proteins comprising the capsid [10]. These factors trigger viral uncoating and release of the infectious genetic material.

Despite their importance, the mechanical properties of viruses remain unexplored, largely due to their extremely small sizes and complex core-shell structure. Experimental techniques such as nanoindentation [11–13] have provided rough estimates of properties of individual viruses. In particular, the Young's modulus E of empty capsids (viruslike particles) of DNA-containing viruses have been estimated at $\approx$1.25 GPa for minute virus of mice (MVM) [11] and $\approx$1.8 GPa for bacteriophage [12], while much lower moduli of ~140–190 MPa have been found for capsids of RNA-containing, cowpea chlorotic mottle virus (CCMV) [13]. The increased rigidity of the DNA-containing capsids, both filled and empty, as compared to their RNA-containing counterparts, is attributed to the need to withstand high internal pressures imposed by tightly packed DNA molecules [14]. Model calculations for the eigenfrequencies of the complete viruses, including the genomic core, usually assume an overall rigidity comparable to benchmark proteins, such as crystalline lysozyme ($E\approx$2.7 GPa) [15]. In general, though, the compliance tensors obtained from a much broader array of viruses, as well as in response to various environments, are necessary to fully understand the mechanical design of these biocolloids.

Inelastic light scattering spectroscopy is a complementary probe technique that allows direct, noncontact, nondestructive measurement of the mechanical properties of the individual unit and its assembly. This technique has been successfully applied to photonic crystals and polymeric nanostructures [16,17] and very recently also to crystals of satellite tobacco mosaic virus (STMV) [18]. In this article we present Brillouin light scattering studies of *Wiseana iridovirus* (WIV) in comparison to assembly of polymeric colloidal particles. In contrast to polymeric colloids, which exhibit only modes localized to individual particles, we discovered that WIV assemblies exhibit propagating phonon modes indicating strong interparticle coupling. Experimental data in-

*Corresponding author. alexei@uakron.edu

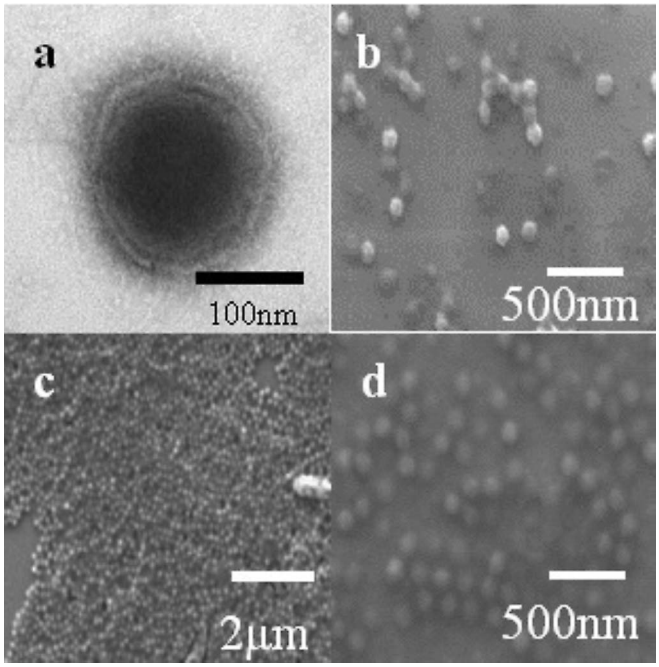

FIG. 1. Electron microscopy images of *Wiseana Iridovirus* (WIV) samples. (a) Transmission electron microscopy image of a single WIV showing the compact DNA core (dark) and the surrounding protein shell. Scanning electron micrographs of (b) scattered single viruses, (c) single-layer of disordered viruses, and (d) expanded view of a single layer showing disordered packing of WIV virions.

dicate surprisingly high modulus of the virus ≈7 GPa, a value representative of a hard plastic rather than a soft rubberlike particle. Results of mechanical modeling agree well with the light scattering data and help to explain the relative contribution of the constituents comprising the core-shell WIV structure.

II. EXPERIMENT AND MODELING

A. Samples

WIV is a large (140 nm outer diameter) icosahedral virus with a 132-nm-diameter double-stranded DNA core surrounded by a ~4-nm lipid bilayer and proteinaceous capsid shell with long fibrils (30 nm) extending from the shell surface [4,19] [Fig. 1(a)]. It has previously been used for responsive photonic crystal assemblies [4] and the core of Au nanoshells [20]. Depending on process conditions, isolated and close-packed assemblies can be fabricated on a variety of substrates [4].

Convective assembly of all samples was performed in a Plas Labs temperature- and humidity-controlled chamber. Virus solutions were taken from a stock solution and centrifuged several times at 4000 rpm and redissolved in Milli-*Q* water to remove buffer and stabilizer from the solution. The virus solution was then adjusted to a final concentration of 10 mg/mL prior to use. Viral films were prepared on silicon substrates. The silicon wafers (Wafer World) and glass slides were cleaned prior to use in a NoChromix solution for 24 h and then washed thoroughly with Milli-*Q* water and dried under a stream of nitrogen. A glass slide was mounted at an angle of 18° from the substrate surface. Ten microliters of colloidal solution was then injected between the substrate and the glass slide. To perform the convective assembly process, a Compumotor motion controller was used to drive the glass slide parallel to the substrate at a fixed rate. Assembly of multilayer virus films occurred at 1 μm/s and 10% relative humidity (R.H.) Single-layer films were generated by convective assembly of the virus solution at 10 μm/s and 15% R.H. Submonolayer films were generated from a 10:1 dilution of the virus solution at 100 μm/s and 10% R.H. After fabrication, the samples were immediately transferred to a controlled environment until needed. All films were imaged using a FEI XL30 scanning electron microscope using 3 kV at a distance of 5 mm (Fig. 1). We also prepared WIV structures on an aluminum mirror, similar to the PMMA colloidal structures (see below). However, a weak Brillouin signal of WIV interfered with the signal coming from scattering on surface modes of Al and these spectra are not analyzed in the current paper.

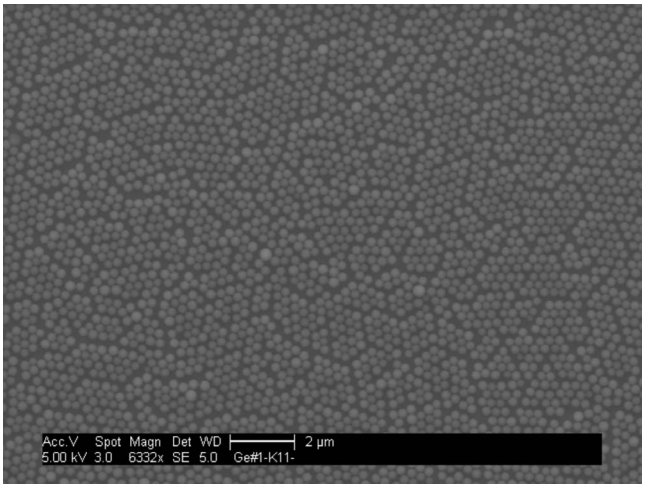

FIG. 2. Scanning electron micrograph of PMMA colloids (D =300 nm) on an aluminum mirror.

PMMA colloidal assembly was studied for comparison because these two colloidal systems (PMMA hard spheres and virus particles) are expected to have similar phononic properties. Three-hundred nanometer PMMA colloids (Polysciences, Inc.) were used as received (2.55% solids in water). A colloidal sample was prepared by the same convective assembly from solution onto clean aluminum mirrors. The substrates were washed successively in ethanol (Fisher) and Milli-*Q* water and then dried under a stream of nitrogen immediately prior to colloid deposition. Assembly occurred at a rate of 10 μm/s at 23 °C and at 15% R.H. The so-obtained assembly of PMMA colloids shows hexagonal close packing with grain boundaries (Fig. 2).

B. Brillouin scattering measurements

Brillouin scattering spectra of the WIV and PMMA assemblies were measured in back-scattering geometry using a tandem Fabry-Perot interferometer (Sandercock model)

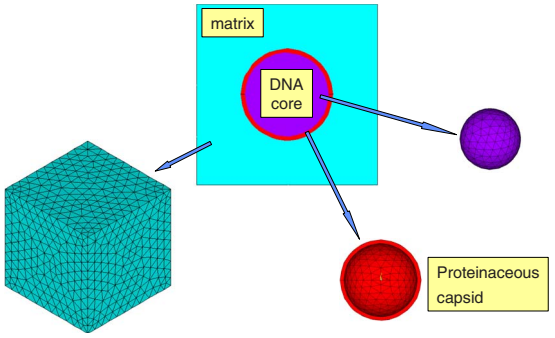

FIG. 3. (Color online) A representative volume element of matrix embedded with a spherical WIV having a DNA core and a capsid shell and its finite element meshes.

and an Ar-ion laser with wavelength $\lambda=514.5$ nm and 10–30 mW power. The free spectral range of the interferometer was set to 30, 50, or 75 GHz. The laser spot size was about 10 μm. The geometry of the measurements was the same as used for analysis of surface waves in thin films [17]. The Brillouin peak positions were estimated by fitting the spectra with Lorentzian curve shapes using ORIGIN (Microcal) software. Samples were measured at different angles $\theta=15°-75°$ between the incident beam and normal to the film surface, the latter oriented horizontally. The change in the angle corresponds to the change in the scattering wave vector Q parallel to the sample surface from 6.3 μm^{-1} to 24 μm^{-1}. Polarization of the incident light was vertical, and no analyzer has been used, except for analysis of PMMA colloids spectra. The samples were measured at room temperature and relative humidities between 20% and 40%.

C. Mechanical modeling

The effective modulus of the virus was calculated (i) analytically using the rule of mixture (ROM) and (ii) numerically using the three-dimensional finite-element (FE) model for micromechanics of composites [21]. The analytical solution was obtained by applying a constant radial strain on the outer surface of the capsid shell. A rule of mixture then leads to an effective bulk modulus of the WIV (k^*):

$$k^* = \frac{k_C k_D}{k_C \mathrm{v}_D + k_D(1-\mathrm{v}_D)}, \tag{1}$$

where $k_i=E_i/3/(1-2\sigma_i)$ with the subscript i representing the D for DNA and C for capsid, and $\mathrm{v}_D=\{r_D/(r_D+t_C)\}^3$ is the volume fraction of the DNA. The effective Young's modulus of WIV (E^*) can then be calculated as

$$E^* = 3(1-2\sigma^*)k^*, \tag{2}$$

where the effective Poisson's ratio of WIV (σ^*) is unknown, but assumed to be 0.33 for consistency with estimates from experiment.

The numerical model considered a representative volume element (RVE) consisting of three phases of materials: the DNA core, the capsid shell, and an arbitrary matrix material surrounding the WIV in the cubic RVE (Fig. 3). Including the third matrix phase eases application of boundary conditions to the FE analysis. The FE calculation was carried out to numerically determine dilute strain concentration tensor (**A**) for a single inclusion of the WIV (DNA+capsid) within the matrix. The tensor **A** was then used to calculate the effective moduli of the composites of the WIV and the matrix by using a Mori-Tanaka method [21,22]. Another FE calculation was conducted by replacing the two-phase WIV with a homogenized single-phase spherical inclusion whose Young's modulus and Poisson's ratio are E^* and σ^*, respectively. While σ^* was assumed to be constant (0.33), E^* varied until the effective moduli of the composites of the homogenized sphere and the matrix coincided with those of the composites of the WIV and the matrix. The properties of the artificial matrix phase introduced in the model influence estimates of the composites moduli. To consider the effect, the Young's modulus of the matrix (E_m) varied from 0.1 GPa to 100 GPa using both two-phase WIV and homogenized sphere inclusions. The deviations of the bulk modulus k^* from the average value in these calculations were less than 1%. The average value of k^* was taken for calculations of the Young's modulus E^* using Eq. (2).

III. RESULTS

In scattering experiments, dependence of vibrational frequency on the scattering wave vector indicates a propagating nature of the vibrational mode, while a Q-independent frequency is usually a sign of a strongly localized mode. It appears that the Brillouin spectra of PMMA and WIV assemblies exhibit strongly different behavior (Figs. 4 and 5). Spectra of PMMA structures exhibit no Q dependence [Figs. 4(a) and 4(b)], indicating strong localization of modes to individual colloidal particles. We were not able to detect any propagating (Q-dependent) mode in PMMA assemblies. This result suggests weak mechanical coupling between colloidal PMMA particles. The three lowest-frequency peaks in PMMA spectra are strongly depolarized [Fig. 4(b)]. The strong rise of intensity in the polarized spectrum of PMMA colloids at $\nu>10$ GHz presents the tail of a longitudinal acousticlike mode localized inside the PMMA particles. It does not show any significant Q dependence and is out of the scope of the current discussion.

In contrast, a strong Q dependence is obvious in the spectra of WIV assemblies [Fig. 4(c)]. Apparently, there is a strong mechanical coupling between the WIV particles that promotes the propagation of acoustic modes. The viral particles have icosahedral symmetry with almost flat surfaces, in contrast to rather spherical shape of PMMA colloidal particles. However, this cannot be the reason for the strong mechanical coupling in the case of WIV because rather long fibrils (~30 nm) will prevent direct mechanical contacts between surfaces of the viral particles. The coupling may arise from entanglement of the fibrillar structures extending from the capsid shell or from long-range charge interactions. Thus the spectra of a thick virus layer is similar to spectra of surface waves in a film, although modes are rather broad and not very intense, most probably due to the inhomogeneous structure of the virus film. The intensity of the surface modes in Brillouin scattering spectra varies with Q due to the selec-

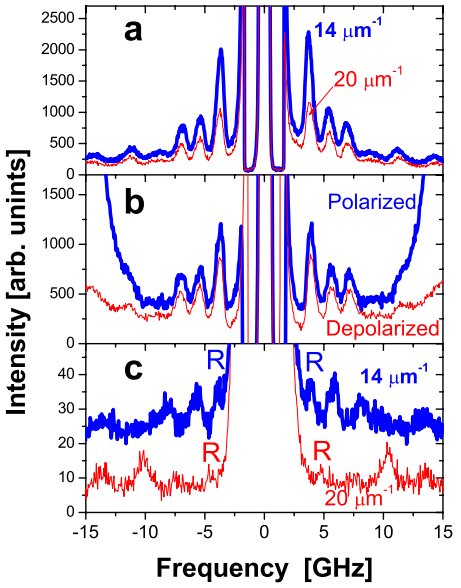

FIG. 4. (Color online) Brillouin scattering spectra at different scattering wave vectors. (a) Spectra of a layer of PMMA colloids measured at $Q=14\ \mu m^{-1}$ (thick blue line) and at $Q=20\ \mu m^{-1}$ (thin red line), no analyzer used. Q-independent peaks indicate vibrational modes localized to individual particles. (b) Spectra of a layer of PMMA colloids measured at $Q=6.3\ \mu m^{-1}$ polarized (thick blue line) and depolarized (thin red line). The rise of the intensity at frequencies above ~10 GHz in the polarized spectrum is the tail of longitudinal acousticlike modes localized inside of PMMA particles. (c) Spectra of a multilayered WIV sample measured at $Q=14\ \mu m^{-1}$ (thick blue line) and at $Q=20\ \mu m^{-1}$ (thin red line), no analyzer used. Q-dependent peaks indicate vibrational modes propagating in the film of the viruses. The lowest-frequency mode (marked by letter R) is the Rayleigh mode. Other modes are higher-order Sezawa modes.

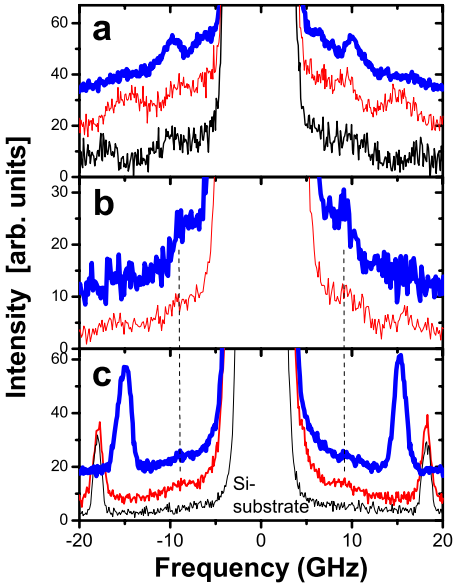

FIG. 5. (Color online) Brillouin scattering spectra of thin WIV structures, no analyzer used. The spectra on each figure are shifted vertically for clarity: (a) Spectra of a single layer of WIV measured at $Q=14\ \mu m^{-1}$ (top spectrum), $Q=20\ \mu m^{-1}$ (middle spectrum) and $Q=24\ \mu m^{-1}$ (lower spectrum). Weak modes exhibit some Q dependence. (b) Spectra of a single layer of WIV measured at $Q=17\ \mu m^{-1}$ (top spectrum) and $Q=20\ \mu m^{-1}$ (lower spectrum). A weak Q-independent mode is visible near 9 GHz. (c) Spectra of a submonolayer of WIV [Fig. 1(b)] measured at $Q=20\ \mu m^{-1}$ (top spectrum) and $Q=24\ \mu m^{-1}$ (middle spectrum) also exhibit Q-independent mode near 9 GHz. The strong peaks at higher frequency are surface Rayleigh mode of Si. Spectrum of Si substrate (lower spectrum) is shown for comparison.

tion rules [24]. We marked the Rayleigh mode (the main mode we will use for the estimates of elastic constants) in Fig. 4(c).

To investigate individual viruses, we analyzed samples of loosely dispersed viruses across a silicon substrate [Fig. 1(b)]. We were able to detect a weak mode in spectra of isolated WIV particles [Fig. 5(c)] where no modes can propagate due to large distances separating the virions [except Si-surface modes clearly visible in the spectra presented in Fig. 5(c)]. This mode seems to be Q independent (Fig. 5), although we need to emphasize that this mode is barely detectable even after extremely long accumulation time. A similar weak mode is also observed in the single-layer sample [Fig. 5(b)]. Spectra of the single layer sample also exhibit weak Q-dependent (propagating) modes [Fig. 5(a)]. Figure 6 presents the dispersion curves for the frequencies of the modes in WIV assemblies at different Q.

Nonpropagating modes observed in the Brillouin spectra are the vibrational eigenmodes of individual particles. High depolarization ratio of these modes in PMMA [Fig. 4(b)] indicates that they are torsional and/or spheroidal type. In that case, the frequency ν_{loc} of the lowest-energy eigenmode for a spherical particle is related to the diameter of the particle D and the transverse sound velocity V_T of the material [23]:

$$\nu_{loc} \cong 0.85\frac{V_T}{D}. \tag{3}$$

Higher-frequency peaks should correspond to higher-order (higher-quantum-number) eigenmodes of a spherical particle. For the purpose of estimating V_T, we analyzed only the lowest-frequency mode in PMMA colloids. Applying Eq. (3) to the spectra of PMMA colloids [Fig. 4(a)], we estimate $V_T=1.38\pm0.05$ km/s from the lowest mode at $\nu\sim3.7$ GHz, in good agreement with values known for bulk PMMA, $V_T=1.41$ km/s [25]. Due to the weak signal, we were not able to analyze the depolarization properties of the Q-independent mode in WIV. We assume that this is the same kind of eigenmode as the strongest mode observed in PMMA colloids. We emphasize that the Q-independent mode in WIV assemblies is much weaker and seems to be not as sharp as in PMMA colloids. This might be explained by a strong damping of the eigenmode in WIV. Applying the same approximation to the WIV eigenmode at $\nu_{loc}=8.8\pm0.2$ GHz (Fig. 6) yields an average transverse sound velocity $V_T=1.45\pm0.05$ km/s; i.e., it appears to be even slightly higher than in a hard plastic like PMMA.

Classical wave theory for a soft film on a hard substrate identifies many different modes (Rayleigh, Sezawa, Longitudinal Guided, etc.) that will appear in the Brillouin scattering

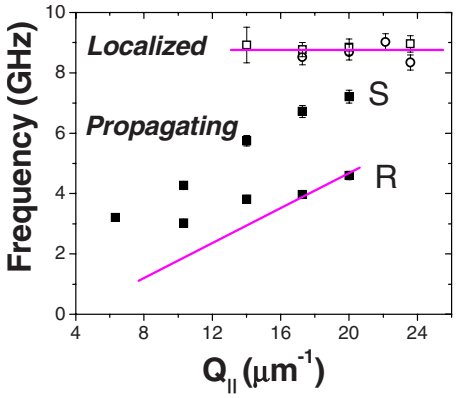

FIG. 6. (Color online) Frequency of Brillouin modes in WIV spectra as a function of the scattering wave vector Q. Q-independent modes are interpreted as localized vibrations from single-layer (open squares) and submonolayer (open circles) WIV assemblies. The average frequency of the localized mode (8.8 ± 0.2 GHz, marked by a solid line) was used in Eq. (3) to estimate transverse sound velocity. Q-dependent modes are propagating surface waves from multilayer WIV structures (solid squares). R marks the Rayleigh mode and S marks the first-order Sezawa mode. The solid line represents the asymptotic value of the Rayleigh velocity at high Q. Error bars represent one standard deviation from averaging positive and negative Brillouin frequency shifts.

spectra. The lowest-frequency propagating mode is the Rayleigh mode traveling along the sample surface. Its frequency ν depends on the Rayleigh velocity V_R and in the high-Q limit ($Qd > 2\pi$, where d is the film thickness) follows the simple relationship [26]

$$\nu = V_R Q / 2\pi. \tag{4}$$

The rigidity of the substrate influences the Rayleigh velocity at lower Q and leads to a deviation from the linear relationship between ν and Q (Fig. 6). Higher-frequency modes in thin films are usually called Sezawa modes. However, in the current paper we focus on the lowest-frequency mode, the Rayleigh mode, because its frequency is sufficient to estimate the rigidity of the WIV. Using Eq. (4) and the data obtained on thick WIV assemblies at high $Q = 17\ \mu\text{m}^{-1}$ and $20\ \mu\text{m}^{-1}$, we estimated the Rayleigh velocity of phonons in the WIV assembly as $V_R = 1.44 \pm 0.1$ km/s (Fig. 6). We did not analyze the propagating modes in thin virus films, because they are in a highly dispersive regime ($Qd < 2\pi$) and their frequencies are significantly affected by elastic properties of the substrate. To determine V_T from the propagating modes, a Poisson's ratio σ must be assumed. For biological objects, this quantity is usually in the range $\sigma = 0.3$–0.4 [12,13] and yields $V_T \approx 1.55 \pm 0.1$ km/s, in good agreement with the estimate obtained from the localized mode. Because the Rayleigh mode is dominated by the shear modulus, any other choice of the Poisson's ratio up to the completely incompressible limit $\sigma = 0.5$ does not affect this estimate significantly. Table I compares sound velocities reported for crystalline lysozyme and DNA with our estimates for WIV. The rigidity of DNA inside of viruses is not known. However, it is known that rigidity of DNA crystals increases significantly with decrease of hydration level [28]. Table I presents the sound velocity in DNA at low hydration levels because we assume that DNA in viral particles is essentially in a dehydrated state. The transverse velocities of WIV are consistent with what would be expected for a DNA containing virus where the rigidity of composite core-shell particle is strongly dominated by its DNA core rather than the capsid shell. Estimates of the rigidity of an empty WIV capsid would help to unravel the role of DNA core. However, empty WIV capsids are not available and we will rely on a model analysis (see below).

TABLE I. Comparison of Brillouin-derived longitudinal and transverse velocities for WIV to biomolecules of WIV and PMMA colloids.

Material	Longitudinal velocity V_L (km/s)	Transverse velocity V_T (km/s)	Density ρ (g/cm^3)	Young's modulus E (GPa)[a]
Lysozyme	1.817 [15,27]	0.915 [15,27]	1.21 [15,27]	2.7
DNA	3.4–3.8 [28]	1.7–1.9[b]	1.21 [28,29]	9.3–11.6[c]
WIV	2.9 ± 0.2[b]	1.45 ± 0.05	1.21 [27]	6.7
PMMA	2.78 [25]	1.41 [25]	1.19 [25]	6.34

[a]Upper limits of Young's modulus calculated from ultrasound velocities.
[b]$V_L \approx 2V_T$ for materials with Poisson's ratio $\sigma \approx 0.33$.
[c]Assuming $\rho = 1.21$ g/cm^3.

To compare our measurements for WIV with previous rigidity studies, Young's modulus E is determined from the transverse sound velocities using

$$E = \rho V_T^2 \left[\frac{3V_L^2 - 4V_T^2}{V_L^2 - V_T^2} \right]. \tag{5}$$

Here V_L is the longitudinal sound velocity and ρ is the average density of a single virion. Overall, the local density within the virus is nonuniform, ranging from the internally packaged DNA to the proteins in the capsid shell. Density of many proteins such as lysozyme are reported to be around $\rho = 1.21$ g/cm^3, where as estimates of DNA and DNA protein complexes range from $\rho = 1.21$ g/cm^3 [27,28] to $\rho = 1.69$ g/cm^3 [29]. Assuming WIV has an outer layer, including lipid bilayer, capsid shell, and surface structure, ≈ 4 nm thick, and the radius of the DNA core is ≈ 66 nm [4,19], the DNA comprises $\approx 83\%$ of the virion by volume. Depending on the density assumed for DNA, the volume average density ranges from 1.21 to 1.6, yielding an estimate for WIV Young's modulus between 6.7 and 8.9 GPa. This is a remarkably high stiffness for a material considered to be "soft matter" and indicates strong influence of the DNA core on the virus modulus.

To provide insight into the relative contribution of DNA core and capsid to the overall rigidity of the virus, the effective modulus of a core-shell sphere was calculated analytically using ROM and numerically using a three-dimensional FE model for micromechanics of composites. The numerical model considered a representative volume element consist-

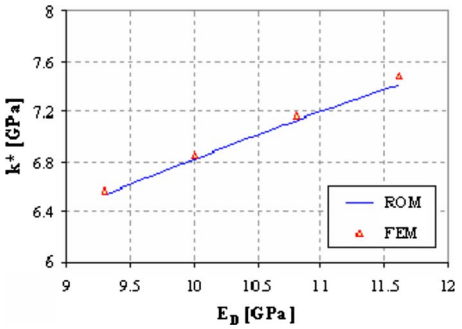

FIG. 7. (Color online) Effective bulk modulus of the whole WIV particle k^* predicted by an analytic solution (ROM) and a numerical method (FEM) assuming different values for the Young's modulus of DNA, E_D.

ing of three phases of materials (Fig. 3). For these calculations, the experimentally measured dimensions and properties were taken as follows: radius of DNA core, r_D=66 nm; thickness of capsid, t_C=4 nm; Young's modulus of DNA, E_D=9.3–11.6 GPa; and Young's modulus of capsid, E_C =2.7 GPa. It was assumed that the Poisson's ratios of DNA (σ_D) and capsid (σ_C) were 0.33.

A comparison between effective bulk modulus of WIV predicted by the analytical (ROM) and numerical (FEM) methods is shown in Fig. 7. The x axis indicates the variation of Young's modulus of the DNA core from 9.3 GPa to 11.6 GPa (expected DNA values, Table I), which resulted in ranges of the WIV bulk modulus (k^*) from 6.6 GPa to 7.5 GPa and Young's modulus (E^*) from 6.8 GPa to 7.9 GPa. These calculations agree fairly well with the experimentally measured value of ~7 GPa and demonstrate that continuum theory provides reasonable estimates of the mechanical properties of a large virus like WIV. Apparently, the effective modulus of the core-shell particle is dominated by variation of the core, since the shell in WIV occupies a relatively small volume.

IV. DISCUSSION

The unexpected observation is the existence of propagating modes in virus assemblies that differentiate them from films of polymeric colloidal particles. The propagating modes appear to be stronger than localized modes in the film of viruses, while no propagating modes have been detected in colloidal PMMA sample. It is interesting to note that propagating modes have been also very recently reported in Brillouin scattering spectra of STM virus crystals [18]. Propagating modes indicate strong mechanical coupling between viruses. The specific origin of this strong particle-particle association is consistent with previous reports indicating difficulty in fabricating uniform, defect-free viral assemblies, especially in comparison to conventional polymer and silica colloids [4]. Close-packed clusters and open aggregate morphology indicate that a reaction-limited association dominates the local morphology of the WIV assemblies [4]. This association provides an important difference between traditional synthetic colloids and biological colloids. The mechanical coupling between virus particles generates assemblies that behave more as a single unit (or film) with local morphological stability and mechanical properties that can be correlated to larger length scales. Post-assembly processing and overall assembly fidelity are enhanced by the coupling between viruses. Despite the strong association between viruses in the assemblies, site-specific heterogeneous surface chemistry is still individualized, a property that is unattainable with other synthetic materials and holds potential for data-storage devices and sensors.

While the Brillouin spectra of viral assemblies provide important information for the use of viruses as device-oriented materials, the properties of individual virus particles provide valuable information to the biological community. Understanding the properties of individual viruses enhances the understanding of the process by which viruses breach cellular membranes during infection and may provide information leading towards new methods to detect, manipulate, or destroy virus particles. While individual polymeric colloidal particles exhibit strong eigenmodes (Fig. 4), very weak signals have been observed for the eigenmodes of individual viruses (Fig. 5). The authors of [18] were not able to detect these modes in crystals of STMV. So the weakness of the eigenmodes seems to be common for different viruses and once again differentiates them from homogeneous polymeric colloidal particles. It is possible that complex core-shell structure of viruses leads to damping of these modes. WIV is almost 10 times larger than STMV and has a diameter closer to the wavelength of light. As a result, WIV modes should scatter light stronger than smaller colloids, and that might be the main reason that the eigenmodes of WIV were detected in our measurements.

The modulus estimated for WIV, $E \approx 7$ GPa, is significantly higher than the values reported for some other viruses. A collection of results for mechanical properties of viruses is summarized in Table II. All values, except STMV and WIV, were estimated using nanoindentation measurements in a fluid environment and FE analysis. A Young's modulus $\approx$1.8 GPa has been initially reported for bacteriophage ϕ29 empty capsid [12]. For an empty capsid of MVM virus, $E \approx 1.25$ GPa has been estimated, and this value increased to $\approx$3 GPa along one of the symmetry axes in MVM containing DNA [11]. The value $E \approx 1$ GPa has been estimated for Murine Leukemia Virus [30]. The softest modulus $E \approx 0.14$–0.19 GPa has been reported for CCMV [13]. Recent theoretical analysis suggests that the quantitative interpretation of these experimental measurements depends significantly on the model approximations [31]. In particular, using a more detailed analysis of the same data, the authors estimated the modulus of bacteriophage ϕ29 to be $E \approx 4.5$ GPa and the modulus of CCMV to be $E \approx 0.28$–0.36 GPa—i.e., 2–2.5 times higher than the original estimates presented in Refs. [12,13]. Brillouin measurements in crystals of STMV were able to measure only longitudinal modes [18]. In that case, knowledge of Poisson ratio is more critical for estimates of the Young's modulus. Assuming $\sigma \approx 0.3$, the authors estimated $E \approx 3.3$ GPa in hydrated STMV crystal [18]. This modulus, however, increases up to $E \approx 10$ GPa in dry STMV crystal. In light of other data for RNA-containing viruses, this value of the Young's modulus is suspiciously

TABLE II. Comparison of data for spherical (icosahedral) viruses: ss and ds mean single stranded and double stranded (RNA or DNA); measured quantities are presented as elastic spring constants in N/m or in measured velocities (V_L, longitudinal sound velocity, and V_T, transverse sound velocity).

Virus, content	Diameter [nm]	Experiment	Conditions	Spring; Velocity	Young's modulus [GPa]	Ref.
MMLV, ssRNA	~85	Nanoindentation	Mature	0.68 N/m	1.027	[30]
		In fluid environment	Immature	0.31 N/m	0.233	
CCMV, ssRNA	~35	Nanoindentation	Empty	0.15–0.19 N/m	0.14–0.19 corrected to 0.28–0.36	[13,31]
		In fluid environment	Full	0.2–0.3 N/m		
STMV, ssRNA	~17	Brillouin (in fluid environment)	Wet	$V_L \sim 1.92$ km/s	3.3	[18]
		Brillouin (dehydrated)	Dry	$V_L \sim 3.43$ km/s	10	
Bacteriophage $\phi 29$, dsDNA	54×42	Nanoindentation	Empty	Bimodal: 0.16 and 0.31 N/m	1.8 corrected to 4.5	[12,31]
		In fluid environment				
MVM, ssDNA	~25	Nanoindentation	Empty	0.58 N/m	1.25	[11]
		In fluid environment	Full	0.6–1.4[a] N/m	1.3–3	
WIV, dsDNA	~140	Brillouin	Full, 20%–40% R.H.	$V_T \sim 1.45$ km/s	~7–8	
		In air with regulated R.H.				

[a]The value depends on the symmetry axis.

high. One of the problems might be related to the assumption of the Poisson's ratio. The authors estimated Young's modulus from the measured longitudinal sound velocity that is dominated by the bulk modulus. In that case the estimate of the Young's modulus depends strongly on the assumed Poisson's ratio. For example, assuming the Poisson's ratio $\sigma \approx 0.33$, the estimate of the Young's modulus [see Eq. (2)] will reduce by ~15%, resulting in $E \sim 2.8$ GPA for hydrated and $E \sim 8.5$ GPa for dry STMV crystals; and assuming $\sigma \approx 0.4$ will lead to reduction of the Young's modulus estimate by ~37%. We note that the assumption of the Poisson's ratio is not so crucial if the shear modulus (transverse sound velocity) is known (our case). This emphasizes a key future experimental challenge to obtaining unambiguous mechanical properties: independent verification of the components of the compliance tensor (or Young's modulus and Poisson's ratio for isotropic particles).

There is a clear difference between our Brillouin scattering data for WIV and earlier nanoindentation estimates (Table II). This difference might have a few reasons.

(i) Experimental techniques and conditions may contribute to this difference. Brillouin spectroscopy measures high-frequency (GHz) modulus, while nano-indentation techniques reflect a lower-frequency response. The rigidity of soft materials is known to exhibit substantial rate dependence, effectively being harder at higher rates of deformation (e.g., PMMA is reported to have a Young's modulus of 3.3 GPa when measured at 10 Hz [32] and 6.3 GPa when measured at GHz frequencies [25]). This difference is associated with relaxation processes that occur in the frequency range between these two measurement frequencies. This point is consistent with high modulus observed for STMV crystals in Brillouin scattering measurements [18].

(ii) In general, the differences may simply reflect the difference of viruses: WIV is substantially (2–5 times) larger than $\phi 29$, CCMV, MMV, and MMLV and thus has a larger rigid genome core. According to our modeling, the volume fraction of DNA is important for overall virus modulus. However, the volume fraction of DNA in WIV is very similar to the smaller DNA virus $\phi 29$, because the capsid thickness of $\phi 29$ is only 1.6 nm compared to ~4 nm in WIV. The DNA core makes up ~83% of the total WIV volume, and it makes up ~81% of the total $\phi 29$ volume. Thus, according to ROM estimates, we should expect a similar modulus for $\phi 29$ and WIV. Unfortunately, only empty $\phi 29$ capsid has been measured. So no comparison to the WIV data is possible.

(iii) The extent of hydration has a considerable influence on compliance, as commonly observed for biological structures. Thus our measurements performed at low levels of hydration might probe viruses that are much harder than the

ones measured in solutions [11–13]. Recent data obtained for STMV [18] indeed indicate a strong dependence of the longitudinal modulus on the level of hydration (Table II).

Only direct comparison of nano-indentation and Brillouin measurements performed on the same virus in similar conditions will help to sort out possible reasons for the observed difference in the modulus estimates. It seems from the nano-indentation data that RNA containing viruses are softer than the DNA containing ones (Table II). Even the empty capsids of an RNA virion have lower spring constants than empty capsids of a DNA virion (Table II). Apparently, nature has developed a shell for DNA capsids capable to withstand the extreme internal pressure of highly packed virial DNA [14], which is usually much stiffer than that of virial RNA. However, Brillouin scattering data do not show a significant difference between the rigidity of RNA-containing STMV and DNA-containing WIV. Detailed analysis of various viruses using both nano-indentation and Brillouin techniques can help to understand the role of capsid structure and core content in overall rigidity and stability of viruses and may provide some indication of relaxation processes.

V. CONCLUSION

In summary, Brillouin spectroscopy is demonstrated as a noncontact and nondestructive method to measure the mechanical properties of viruses and their assemblies, complementing alternative probe techniques. The results demonstrate strong mechanical coupling between individual WIV particles and their surprisingly high modulus of ≈ 7 GPa. Mechanical modeling confirmed that the hard DNA core dominates the modulus. We emphasize that the Brillouin technique might find broad application in analyses of the mechanical properties of biological structures and other soft materials assemblies, their dependence on environment, and interactions. Furthermore, knowledge of the mechanical properties of viruses and their assemblies and knowledge of their vibrational eigenmodes (phononics) might help to model drug and gene delivery processes, to address some antiviral therapy approaches, define processing limitations of viral nanotemplates and devices and provide insight into the dynamic behavior of viruses throughout their lifetime.

ACKNOWLEDGMENTS

The Akron team appreciates financial support from AFRL and AFOSR through the Cooperative Center in Polymer Photonics. R.D.H. thanks the NSF for support and J.N. thanks the NSF REU program for the financial support.

[1] T. Douglas and M. Young, Science **312**, 873 (2006).
[2] T. Lin, J. Mater. Chem. **16**, 3673 (2006).
[3] A. Nedoluzhko and T. Douglas, J. Inorg. Biochem. **84**, 233 (2001).
[4] S. B. Juhl, E. P. Chan, Y. Ha, M. Maldovan, J. Brunton, V. Ward, T. Dokland, J. Kalmakoff, B. Farmer, E. L. Thomas, and R. A. Vaia, Adv. Funct. Mater. **16**, 1086 (2006).
[5] M. L. Flenniken, L. O. Liepold, B. E. Crowley, D. A. Willits, M. J. Young, and T. Douglas, Chem. Commun. (Cambridge) **4**, 447 (2005).
[6] Q. Wang, T. W. Lin, J. E. Johnson, and M. G. Finn, Chem. Biol. **9**, 813 (2002).
[7] R. J. Tseng, C. L. Tsai, L. P. Ma, and J. Y. Ouyang, Nat. Nanotechnol. **1**, 72 (2006).
[8] P. J. Yoo, K. T. Nam, J. F. Qi, S. K. Lee, J. Park, A. M. Belcher, and P. T. Hammond, Nat. Mater. **5**, 234 (2006).
[9] K. T. Nam, D. W. Kim, P. J. Yoo, C. Y. Chiang, N. Meethong, P. T. Hammond, Y. M. Chiang, and A. M. Belcher, Science **312**, 885 (2006).
[10] A. E. Smith and A. Helenius, Science **304**, 237 (2004).
[11] C. Carrasco, A. Carreira, I. A. T. Schaap, P. A. Serena, J. Gómez-Herrero, M. G. Mateu, and P. J. de Pablo, Proc. Natl. Acad. Sci. U.S.A. **103**, 13706 (2006).
[12] I. L. Ivanovska, P. J. de Pablo, B. Ibarra, G. Sgalari, F. C. MacKintosh, J. L. Carrascosa, C. F. Schmidt, and G. J. L. Wuite, Proc. Natl. Acad. Sci. U.S.A. **101**, 7600 (2004).
[13] J. P. Michel, I. L. Ivanovska, M. M. Gibbons, W. S. Klug, C. M. Knobler, G. J. L. Wuite, and C. F. Schmidt, Proc. Natl. Acad. Sci. U.S.A. **103**, 6184 (2006).
[14] D. E. Smith, S. J. Tans, S. B. Smith, S. Grimes, D. L. Anderson, and C. Bustamante, Nature (London) **413**, 748 (2001).
[15] M. Talati and P. K. Jha, Phys. Rev. E **73**, 011901 (2006).
[16] W. Cheng, J. Wang, U. Jonas, G. Fytas, and N. Stefanou, Nat. Mater. **5**, 830 (2006).
[17] R. D. Hartschuh, A. Kisliuk, V. Novikov, A. P. Sokolov, P. R. Heylieger, C. M. Flannery, W. L. Johnson, C. L. Soles, and W. L. Wu, Appl. Phys. Lett. **87**, 173121 (2005).
[18] B. Stephanidis, S. Adichtchev, P. Gouet, A. McPherson, and A. Mermet, Biophys. J. **93**, 1354 (2007).
[19] X. Yan, N. H. Olson, J. L. Van Etten, M. Bergoin, M. G. Rossmann, and T. S. Baker, Nat. Struct. Biol. **7**, 101 (2000).
[20] C. Radloff, R. A. Vaia, J. Brunton, V. Ward, J. Kalmakoff, and T. Dokland, Proc. SPIE **5592**, 143 (2005).
[21] T. Mori and K. Tanaka, Acta Metall. **21**, 571 (1973).
[22] Y. A Benveniste, Mech. Mater. **6**, 147 (1987).
[23] E. Duval, A. Boukenter, and B. Champagnon, Phys. Rev. Lett. **56**, 2052 (1986).
[24] J. R. Sandercock, Phys. Rev. Lett. **29**, 1735 (1972).
[25] K. Weishaupt, H. Krbecek, M. Pietralla, H. D. Hockhheimer, and P. Mayr, Polymer **36**, 3267 (1995).
[26] F. Nizzoli and J. R. Sandercock, in *Dynamical Properties of Solids*, edited by G. K. Horton and A. A. Maradudin (Elsevier, Amsterdam, 1990), Vol. 6, pp. 281–335.
[27] M. Tachibana, K. Koyima, R. Ikuyama, Y. Kobayashi, and M. Ataka, Chem. Phys. Lett. **332**, 259 (2000).
[28] S. A. Lee, S. M. Lindsay, J. W. Powell, T. Weidlich, N. J. Tao, and G. D. Lewen, Biopolymers **26**, 1637 (1987).
[29] G. D. Fasman, *Handbook of Biochemistry and Molecular Bi-*

ology, 3rd ed. (CRC Press, Cleveland, 1975), Vol. 1, pp. 560–568.

[30] N. Kol, M. Gladnikoff, D. Barlam, R. Z. Shneck, A. Rein, and I. Rousso, Biophys. J. **91**, 767 (2006).

[31] M. M. Gibbons and W. S. Klug, Phys. Rev. E **75**, 031901 (2007).

[32] W. Wunderlich, in *Polymer Handbook*, 3rd ed., edited by J. Brandrup, E. H. Immergut, and E. A. Grulke (Wiley, New York, 1989), pp. 77–80.